Electronic Supplementary Material (ESI) for Physical Chemistry Chemical Physics.

Supplementary information

Investigating thermal removal steps of capping agents in the synthesis of bimetallic iridium-based catalysts for the ethanol oxidation reaction

Carolin Prössl, Markus Kübler, Mohammed A. Nowroozi, Stephen Paul, Oliver Clemens, Ulrike I. Kramm

SI content

Experimental part related to the applied characterization techniques.

Fig. S1: Optimisation of the Ir:Me ratio for IrSn (**a**, **b**) and IrNi (**c**, **d**) catalysts with respect to EOR.

Fig. S2: Effect of cleaning steps on particle size distribution for **a)** IrSn and **b)** IrNi catalysts, and TEM images of **c)** IrSn after H_2 cleaning step and **d)** IrNi after H_2 cleaning step.

Fig. S3: XP spectra of the Ir 4f (a), Sn 3d (b), and O 1s (c) finescan regions of the **IrSn** catalysts after different treatment steps.

Fig. S4: XP spectra of the Ir 4f (a), Ni 2p (b), and O 1s (c) finescan regions of the **IrNi** catalysts after different treatment steps.

Fig. S5: Change in chemical states of Ir and Sn for IrSn catalysts (a) and for Ir and Ni in IrNi catalysts (b) as well as relation between ECSA and Ir^0 content (c) and ECSA and Ir^{4+} content (d).

Table S1: Surface atomic composition of the **IrSn** (a) and **IrNi** (b) catalysts from XPS and Ir loading from EDS. The calculated weight percentage of metals on carbon is 50 wt%, based on this a weight ratio of (Ir+Me)/C of 1.0 is anticipated.

Table S2: Lattice parameter *a* and volume weighted average column length $L_{vol\ IB}$ and related mass fraction as extracted from XRD (compare Fig. 1, main manuscript) using the Rietveld method for fitting.

Table S3: Band assignment for the FT-IR spectra shown in Fig. 3 (main manuscript).

Experimental

Electrochemical Characterization

The electrochemical experiments in terms of cyclic voltammetry were conducted with a potentiostat Nordic Electrochemistry ApS ECi-200 controlled by the software Nordic Electrochemistry ApS EC4^{TM}DAQ.

Electrode preparation: The catalyst ink was mixed from 5 mg catalyst in 25 µL Nafion® solution, 500 µL ethanol and 2500 µL deionized water for twice 15 min in the ultrasonic bath, 3 min in the vortex shaker and a final treatment with the ultrasonic homogenizer (Hielscher UP50H). An aliquot of 10 µL ink was dropped onto the polished glassy carbon electrode and air-dried to obtain a catalyst loading of 84.2 µg cm^{-2}, corresponding to a metal loading of 42.1 µg cm^{-2} (considering the anticipated loading of 50 wt%). The electrochemical setup includes a glassy carbon disc as working electrode with an area of A = 0.1963 cm², an alkaline Hg | HgO | 1 M NaOH reference electrode (RE-61AP, ALS Co., Ltd) and a gold rod or glassy carbon counter electrode. To reference the Hg | HgO | 1 M NaOH electrode in respect to the reversible hydrogen electrode (RHE) potential a hydrogen reference electrode (HydroFlex, gaskatel) was used. All given potentials in this paper refer to the RHE.

Electrochemical conditioning and ECSA calculation: The initial **IrSn** and **IrNi** catalysts without any cleaning were subjected to an electrochemical cleaning protocol adapted from Yang *et al*.[1] prior to the conditioning. During the electrochemical cleaning protocol, the electrode is cycled 100 times in 0.5 M NaOH with a scan rate of 500 mV s^{-1} between 0.0–0.8 V_{RHE} and rinsed with DI water. The standard catalyst activation, all catalysts were subjected to, consisted of 50 cycles with 200 mV s^{-1}, 10 cycles with 100 mV s^{-1}, 2 cycles with 50 mV s^{-1}, 2 cycles with 20 mV s^{-1} and 2 cycles with 10 mV s^{-1} in a potential window of 0.06–1.0 V_{RHE} in 100 mL N_2-purged 0.1 M KOH solution. The data evaluation of the electrochemical surface area was performed with the software Nordic Electrochemistry ApS EC4^{TM}View (version: 1.2.55), assuming a theoretical charge per unit area of Q_H^S = 218 µC cm^{-2} and a fractional hydrogen coverage of Θ=0.65 for an endpoint potential of 0.06 V_{RHE}.[2] The integrated area was calculated from the cyclic voltammogram with 10 mV s^{-1} as difference curve. The double layer capacitance was assumed constant over the potential region of hydrogen adsorption. The correction was performed by creating a straight baseline at the minimum of the double layer region at 0.36–0.46 V_{RHE}. The ECSA was calculated with the following equation (2):

$$ECSA = \frac{Q_H}{\theta\, Q_H^S} \qquad \text{Eq. (1)}$$

EOR activity measurement: By addition of 2925 µL ethanol to 100 mL 0.1 M KOH a solution of 0.5 M ethanol was obtained. The activity for EOR was evaluated by 2 cycles with 100 mV s^{-1}, 1 cycle with 50 mV s^{-1}, 1 cycle with 20 mV s^{-1} and 2 cycles with 10 mV s^{-1}. Any values extracted from polarization curves with 10 mV s^{-1} were capacity-corrected by subtracting the CV in N_2-saturated electrolyte with 10 mV s^{-1}.

Structural Characterization

TEM and EDS: TEM and EDS as well as the identic location (IL) measurements were obtained at an electron microscope (model: CM 20 ST, FEI) equipped with a LaB_6 filament emitter and a resolution of 2.3 Å. The samples were prepared by depositing a catalyst dispersion in ethanol on carbon-coated copper or gold finder grids. The images were taken in bright field mode at 200 kV acceleration voltage with a CCD camera. The evaluation of particle sizes and morphology was done with ImageJ Software (version: 1.52a).

The local chemical composition of the samples was obtained by EDS (for 60 s) and quantified using the software INCA (version: 4.15, Oxford Instruments) with a typical precision of ±5 %.

X-ray Diffraction: The analysis of crystallinity and phase composition by XRD was carried out with a Bruker-AXS D8 Advance-diffractometer with a VÅNTEC detector. The source of Cu-K_α-radiation (λ = 1.5406 Å) was operating at an acceleration voltage of 30 kV and 40 mA anodic current. The diffractograms were recorded in Bragg-Brentano geometry on Si low background sample holders within an angular range of 2ϑ = 20°–130° with a step size of 0.0066°, a scan rate of 0.02 s per step and a fixed divergence slit of 0.3°. The obtained data were fitted using the Rietveld method as implemented in the software TOPAS 6 (Bruker AXS, Karlsruhe, Germany). The instrumental intensity function was determined empirically from a fundamental parameters set by using a reference scan of a LaB_6 standard (NIST 660a).

FT-IR: FT-IR spectra were recorded with a PerkinElmer Spectrum One FT-IR spectrometer in attenuated total reflection (ATR) mode from 4000–650 cm^{-1}. (The device was equipped with a single reflection PerkinElmer UATR unit.) Each individual spectrum was obtained by accumulation of 10 scans with a resolution of 1 cm^{-1}.

X-ray Photoelectron Spectroscopy: XPS were measured with a hemispherical analyser (model: PHOIBOS 150, SPECS Surface Nano Analysis GmbH) in constant energy mode using monochromatic Al-K_α radiation (E = 1.4867 keV, line width = 0.85 eV) (model: XR50M, SPECS Surface Nano Analysis GmbH) as x-ray source. The spectra were obtained with an extended range channel electron multiplier detector (model: CEM 9 Channeltron, SPECS Surface Nano

Analysis GmbH). Survey scans were collected with an energy step of 0.5 eV and a pass energy of 30 eV and high-resolution scans for C 1s, O 1s, Sn 3d, Ni 2p, In 3d, Ir 4f with 0.05 eV at pass energies of 10 eV (5 eV for Sn 3d, Ni 2p). Quantification of the spectra was performed with CasaXPS (version: 2.3.16, Casa Software Ltd) offering a typical accuracy of ±10 %. For the high-resolution scans a Shirley background was adapted to account for inelastic electron scattering and the signals deconvoluted with mixed Gaussian/Lorentzian (70/30) line shapes. The fitted peak areas were corrected by atomic sensitivity factors implemented in the software. The samples were pressed as powder on indium foil and therefore, the oxygen 1s peak was corrected for the In-O and In-OH contribution.

Carbon is the main component of the catalysts and is a composite of the graphene layers (C=C, sp^2), amorphous and aliphatic fractions (C-H sp^3) and a variation of heteroatom compounds (C-O, C-N, C=O, O-C=O). The O 1s peak was assigned to lattice metal oxide (Me-O) with Ir or In, metal or organic hydroxyl (Me-OH, C-OH), ether bound and carbonyl (C-O, C=O), carboxyl (O-C=O) and adsorbed water. A monodentate binding OAc is included in the C-O, C=O species and bidentate OAc in the O-C=O species of the O 1s peak. The Ir 4f doublet was fitted with a peak separation of 2.9 eV and equal FWHM with Ir^0 and Ir^{4+} species. For the quantification only the $4f_{7/2}$ contribution was evaluated. Three Sn species, metallic (Sn^0) and two oxides (Sn^{2+}, Sn^{4+}) were taken into account for fitting the Sn $3d_{3/2}$ peak. XPS spectra of mixed Ni components are a complex combination of multiplet splitting, shake-up and plasmon loss structures.[3] A fit of three main species, metallic (Ni^0), oxides (Ni^{2+}) and hydroxides (Ni^{2+}, Ni^{3+}), was applied with additional peaks shifted to the main peak. Due to the low resolution of the Ni fine spectra the species assignment must be taken with caution.

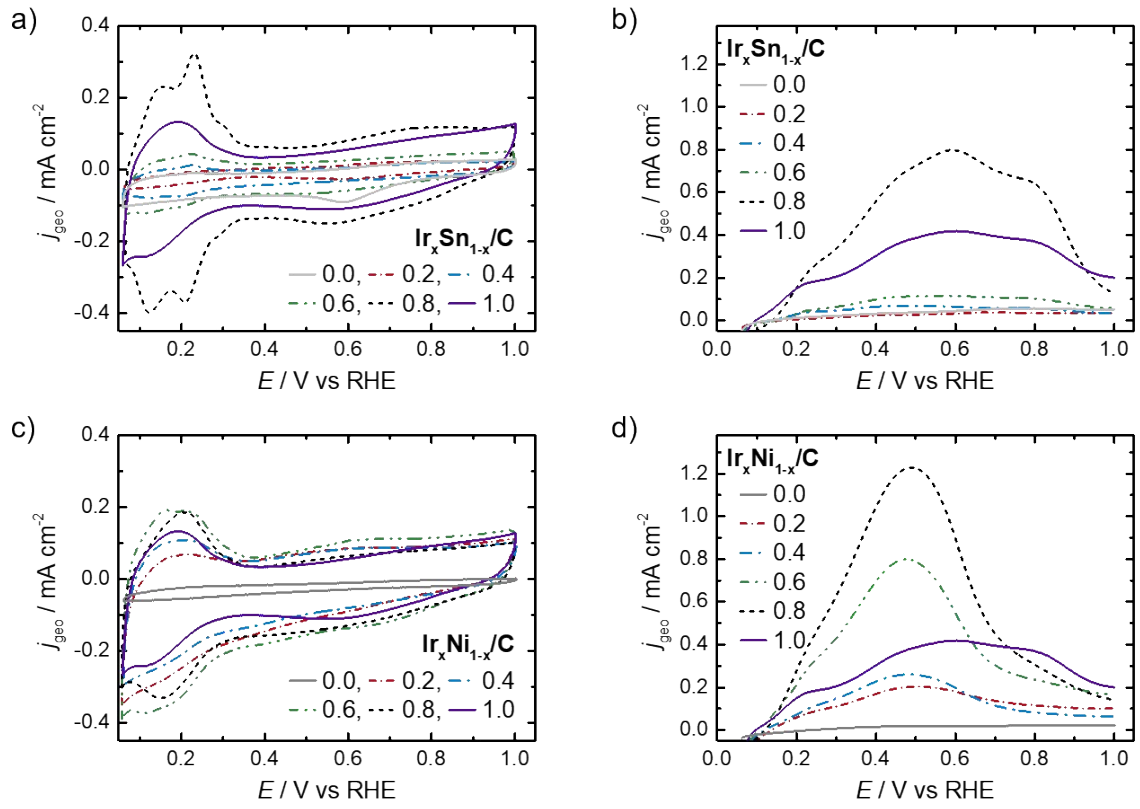

Fig. S1: Optimisation of the Ir:Me ratio for IrSn (**a**, **b**) and IrNi (**c**, **d**) catalysts with respect to EOR. In **a** and **c** the cyclic voltammetry in 0.1 M KOH is shown and in **b** and **d** the measurements of EOR activity after addition of 0.5 M EtOH in 0.1 M KOH (N_2-sat, 10 mV s^{-1}, 84 µg cm^{-2} catalyst loading). For the Ir_xMe_{1-x} catalysts, the nominal x value from the synthesis is indicated.

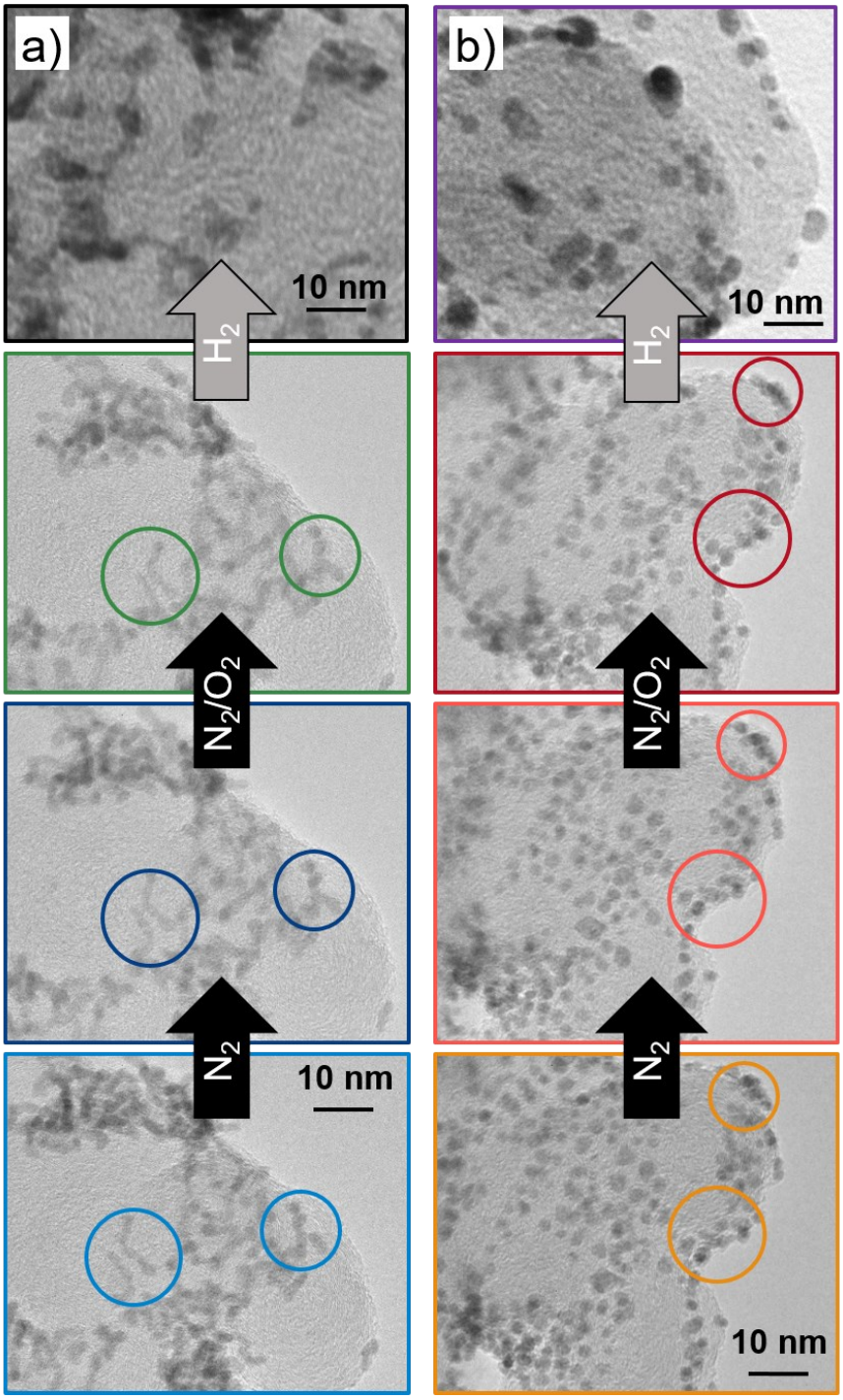

Fig. S2: IL-TEM micrographs of the initial (a) **IrSn_N°2** ($Ir_{0.7}Sn_{0.3}$) and (b) **IrNi** ($Ir_{0.9}Ni_{0.1}$) catalysts and with subsequent cleaning steps under N_2 and N_2/O_2. The circles are indicating characteristic areas. In case of H_2 treatment step conventional TEM images are shown. Also, for the initial catalyst a second particle size distribution from conventional TEM was determined that gave similar results (IrSn initial: 1.7 ± 0.5 nm and IrNi initial: 2.0 ± 0.5 nm).

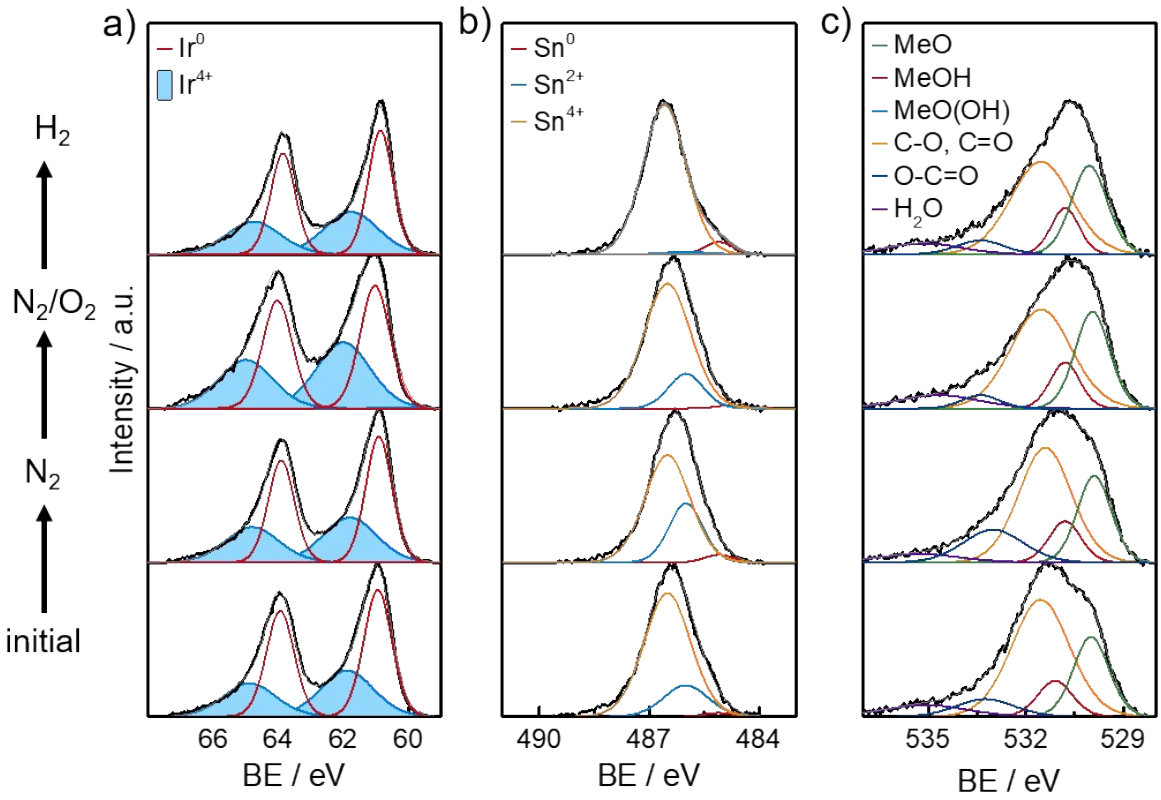

Fig. S3: XP spectra of the Ir 4f (a), Sn 3d (b), and O 1s (c) finescan regions of the **IrSn** catalysts after different treatment steps. Deconvolution and species assignment according to the experimental section.

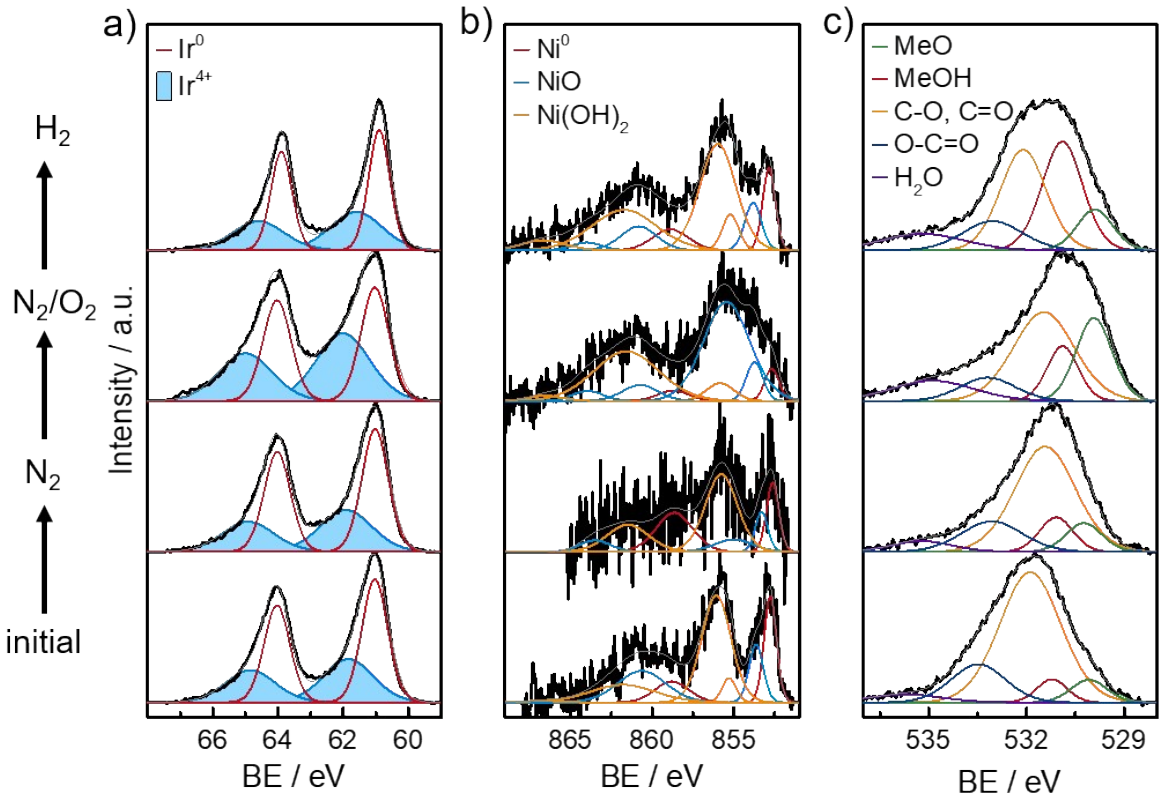

Fig. S4: XP spectra of the Ir 4f (a), Ni 2p (b), and O 1s (c) finescan regions of the **IrNi** catalysts after different treatment steps. Deconvolution and species assignment according to the experimental section.

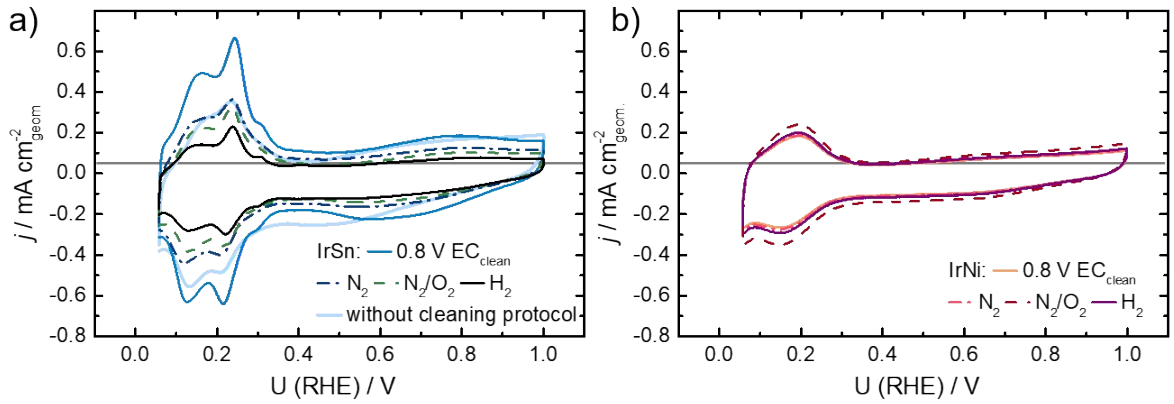

Fig. S5: Cyclic voltammograms with current densities related to the geometric area of the RDE electrode of **IrSn** (a) and **IrNi** (b) catalysts after corresponding cleaning steps in N_2-saturated 0.1 M KOH with a sweep rate of 10 mV s^{-1} and 84 µg cm^{-2} catalyst loading. As indicated, the initial catalysts were investigated after previously being submitted to fast potential sweeps between 0.0–0.8 V_{RHE} in 0.5 M NaOH. For reasons of comparison the CV of the IrSn sample measured without cleaning is shown as well. All displayed CVs are taken after activation scans between 0.06–1.0 V_{RHE} (see Experimental part for details).

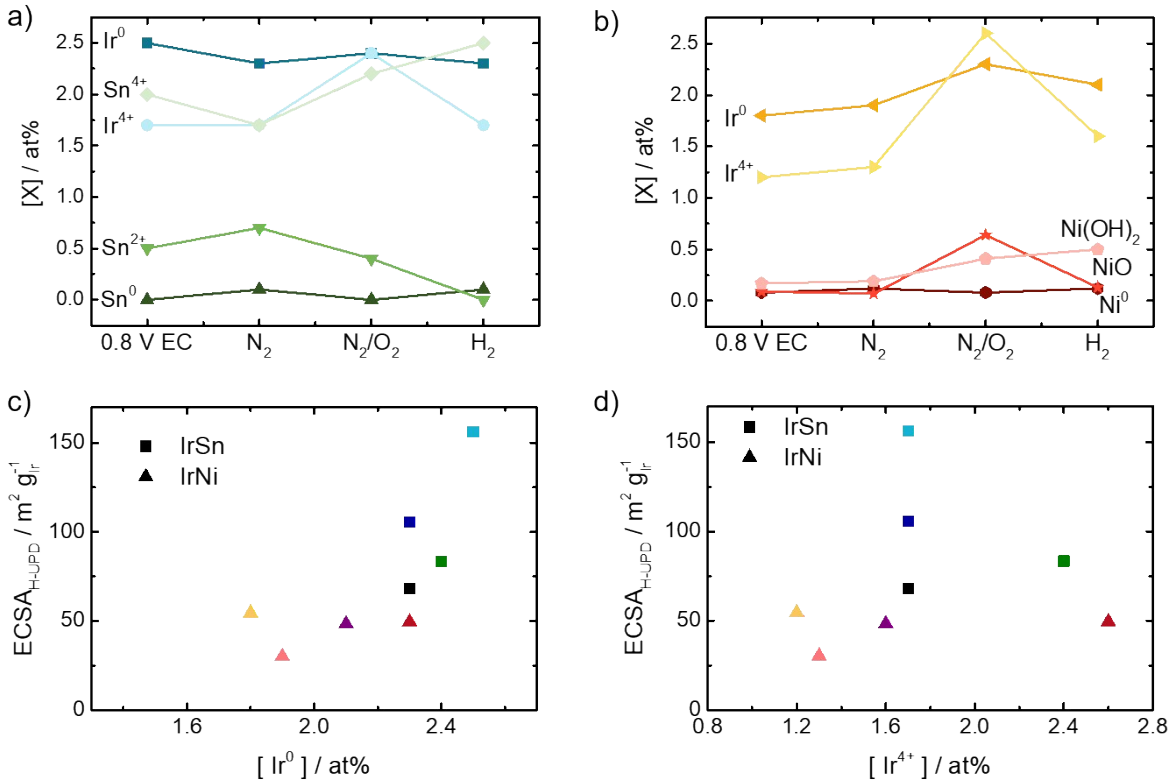

Fig. S6: Change in chemical states of Ir and Sn for IrSn catalysts (a) and for Ir and Ni in IrNi catalysts (b) as well as relation between ECSA and Ir^0 content (c) and ECSA and Ir^{4+} content (d).

Table S1: Surface atomic composition of the **IrSn** (a) and **IrNi** (b) catalysts from XPS and Ir loading from EDS. The calculated weight percentage of metals on carbon is 50 wt%, based on this a weight ratio of (Ir+Me)/C of 1.0 is anticipated.

a) Sample	Sn /at. %	Ir /at. %	O /at. %	C /at. %	Ir /wt. % XPS	Wt-ratio (Ir+Sn)/C	Ir /wt. % EDS
IrSn_Nº2	1.6	3.7	11.8	82.9	34.0	0.91	23.3
IrSn	2.5	4.2	12.8	80.6	35.4	1.14	
IrSn-N_2	2.4	3.9	12.4	81.2	34.1	1.06	
IrSn-N_2/O_2	2.6	4.8	16.0	76.5	38.4	1.34	
IrSn-H_2	2.6	3.8	11.3	82.3	33.0	1.05	

b) Sample	Ni /at. %	Ir /at. %	O /at. %	C /at. %	Ir /wt. % XPS	Wt-ratio (Ir+Ni)/C	Ir /wt. % EDS
IrNi_Nº2	0.4	2.2	7.3	90.1	25.5	0.41	16.6
IrNi	0.3	3.1	10.9	85.7	32.5	0.60	17.3 (IL)
IrNi-N_2	0.4	3.2	10.6	85.8	33.7	0.62	17.2 (IL)
IrNi-N_2/O_2	1.1	4.9	16.3	77.6	42.9	1.08	20.2 (IL)
IrNi-H_2	0.7	3.5	8.6	87.1	35.7	0.68	-

Table S2: Lattice parameter *a* and volume weighted average column length $L_{vol\ IB}$ (also assigned as crystallite size) and related mass fraction as extracted from XRD (compare Fig. 1) using the Rietveld method for fitting (Errors are given in parenthesis, f denotes a fixed value).

a) sample	a / Å	$L_{vol\ IB}$ / nm	wt%	a / Å	$L_{vol\ IB}$ / nm	wt%
IrSn	3.903 (5)	1.3 (1)	100			
IrSn-N_2	3.888 (4)	1.5 (1)	100			
IrSn-N_2/O_2	3.848 (7)	1.1 (1)	100			
IrSn-H_2	3.863 (2)	1.8 (1)	96.9	4.096 (1)	42.2 (2)	3.1

b) sample	a / Å	$L_{vol\ IB}$ / nm	wt%	a / Å	$L_{vol\ IB}$ / nm	wt%
IrNi	3.839 (f)	1.1 (1)	73.8	3.662 (4)	2.2 (1)	26.2
IrNi-N_2	3.839 (f)	1.1 (1)	79.15	3.677 (3)	2.5 (2)	20.85
IrNi-N_2/O_2	3.838 (2)	2.4 (1)	100			
IrNi-H_2	3.832 (1)	2.6 (1)	100			

Table S3: Band assignment for the FT-IR spectra shown in Fig. 3.

Band / cm^{-1}	Assignment	Reference
3040-3010 broad	ν(=C-H)	[4]
2950 shoulder	$\nu_{as}(C\text{-}H_3)$	[5]
2905 s	$\nu_{as}(C\text{-}H_2)$ of OAc capped NP	[6-8]
2840 s	$\nu_{s}(C\text{-}H_2)$ of OAc capped NP	[6-8]
2200-2280	aromatics of Vulcan	reference spectra (not shown)
2125-2085	aromatics of Vulcan	reference spectra (not shown)
1995-1985	aromatics of Vulcan	reference spectra (not shown)
1530-1540 s	ν_{as}(COO-Me) of OAc capped NPs	[5, 6, 8-11]
1440 w	ν_{s}(COO-Me) of OAc capped NPs	[5, 6, 8-11]

References

1 H. Yang, Y. Tang and S. Zou, *Electrochemistry Communications*, 2014, **38**, 134–137.
2 R. Woods, *Journal of Electroanalytical Chemistry and Interfacial Electrochemistry*, 1974, **49**, 217–226.
3 M. C. Biesinger, B. P. Payne, L. W. M. Lau, A. Gerson and R. C. St. Smart, *Surface and Interface Analysis*, 2009, **41**, 324–332.
4 N. Shukla, C. Liu, P. M. Jones and D. Weller, *Journal of Magnetism and Magnetic Materials*, 2003, **266**, 178-184.
5 Y. Lu and J. D. Miller, *Journal of Colloid and Interface Science*, 2002, **256**, 41-52.
6 H. G. Bagaria, E. T. Ada, M. Shamsuzzoha, D. E. Nikles and D. T. Johnson, *Langmuir*, 2006, **22**, 7732-7737.
7 D. Li, C. Wang, D. Tripkovic, S. Sun, N. M. Markovic and V. R. Stamenkovic, *ACS Catalysis*, 2012, **2**, 1358–1362.
8 L. Zhang, R. He and H.-C. Gu, *Applied Surface Science*, 2006, **253**, 2611-2617.
9 C. W. Kim, H. G. Cha, Y. H. Kim, A. P. Jadhav, E. S. Ji, D. I. Kang and Y. S. Kang, *The Journal of Physical Chemistry C*, 2009, **113**, 5081-5086.
10 I. O. Perez De Berti, M. V. Cagnoli, G. Pecchi, J. L. Alessandrini, S. J. Stewart, J. F. Bengoa and S. G. Marchetti, *Nanotechnology*, 2013, **24**, 175601.
11 X. Wang, K. Han, F. Wan, Y. Gao and K. Jiang, *Materials Letters*, 2008, **62**, 3509-3511.